Developmental timing of tumor initiation determines treatment response and cellular composition of medulloblastoma

By
Daniel Malawsky

Senior Honors Thesis
Biostatistics
University of North Carolina at Chapel Hill

April 16th, 2020

Approved:

Professor Timothy Gershon,
Thesis Advisor

Professor Yun Li,
Departmental Advisor

Professor Yuchao Jiang,
Reader

Introduction

Medulloblastoma is the most common malignant pediatric brain tumor (1). Medulloblastomas are formed in the cerebellum and have been resolved into four subtypes in humans: Sonic Hedgehog (SHH), WNT, group 3, and group 4. These designations have been developed using a variety of biological markers, including bulk transcriptomic and genetic analyses. However, within each of these 4 designations, clinical outcomes remain heterogeneous, suggesting that there are differences between tumors within a given subtype (2). Further stratification of each subtype is necessary in order to better tailor treatments and predict clinical outcomes.

The SHH subtype of medulloblastoma is driven by the aberrant proliferation of cells via the SHH pathway. The SHH signaling pathway is essential in the development of the central nervous system (3). Canonically, the pathway is activated when the glycoprotein Shh binds the transmembrane protein Patched1 (Ptch1) (fig.1). Ptch1 binds the G-protein coupled receptor-like protein Smoothened (Smo), however, binding of Shh dissociates Ptch1 from Smo relieving inhibition. Smo then accumulates at the primary cilium and initiates the signaling cascade. The cascade results in the translocation of the Gli2 transcription factor protein into the nucleus. Gli2 upregulates the transcription of target genes including Ccnd1, Myc, and Gli1 resulting in a positive feedback loop and increased proliferation. In SHH medulloblastomas, tumor cells evade inhibition of the SHH pathway.

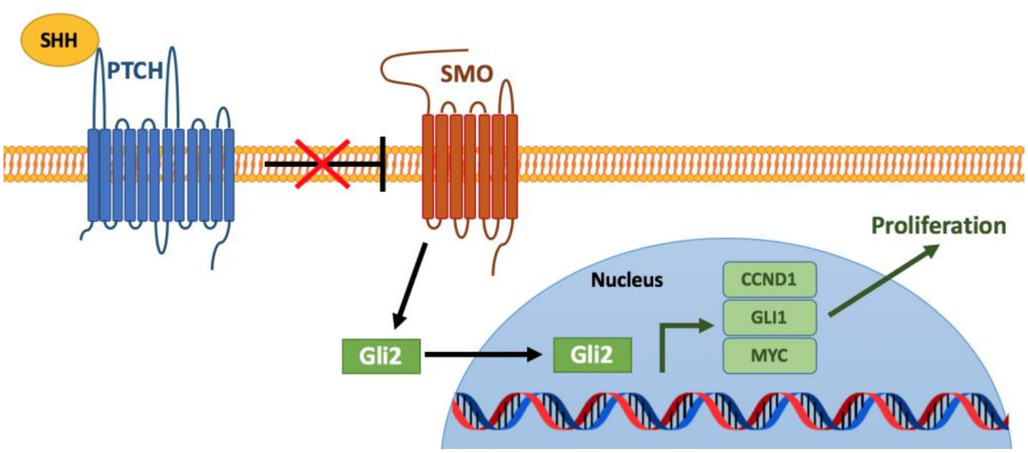

Figure 1. The Sonic Hedgehog Pathway. Shh protein binds Ptch1 which releases Smo, leading to a signaling cascade that translocates Gli2 into the nucleus, upregulating transcription of *Ccnd1*, *Gli1*, and *Myc* and proliferation.

Cerebellar granule neuron progenitors (CGNPs) have been identified as the proximal cells of origin for medulloblastomas in genetically-engineered mice (4). However, mouse studies have shown that aberrant hyperactivation of the SHH pathway in both more primitive neural stem cells of the Gfap lineage as well as in more committed CGNPs of the Math1 lineage results in the development of SHH medulloblastomas (5,6). Pathological and bulk transcriptomic analyses show these tumors to be similar to each other, but mice with tumors initiated in neural stem cells have a shorter survival time (5,6). In humans, it has been reported that age of onset is a predictor of clinical outcomes, again suggesting a role for developmental timing of tumor initiation in determining the malignancy of a tumor (2). These observations led us to hypothesize that the timing of tumor initiation plays a determining role in the cellular composition of medulloblastomas resulting in differential responses to treatment.

Results

Differential survival rate and response to radiation therapy between medulloblastomas from progenitors or stem cells

To induce medulloblastoma formation, we bred *SmoM2* mice, which contain a mutant Cre-dependent Smo gene that is constitutively expressed once activated (7), with *Math1-Cre* or *hGfap-Cre* mice that express Cre-recombinase in cells of the *Math1* or *Gfap* lineage, respectively. The mutant Smo gene is not native to mice and therefore is not inhibited by the mouse Smo inhibitor protein Ptch1, resulting in constitutive activation of the SHH pathway. As *Math1* is expressed in CGNPs, the *Math1-Cre/SmoM2* (*M-Smo*) mice develop medulloblastomas with CGNPs as the cell of origin (8). In contrast, *Gfap* is expressed in central nervous system stem cells (9), leading *hGfap-Cre/SmoM2* (*G-Smo*) mice to develop medulloblastomas with neural stem cells as the cell of origin. All *M-Smo* and *G-Smo* mice develop medulloblastomas. Although they both develop SHH-driven medulloblastomas, *M-Smo* mice live significantly longer than *G-Smo* mice without treatment (fig. 2a). Radiation therapy extends the survival time of *M-Smo* mice (fig. 2b) while radiation therapy has no observed effect on survival in *G-Smo* mice (fig. 2c).

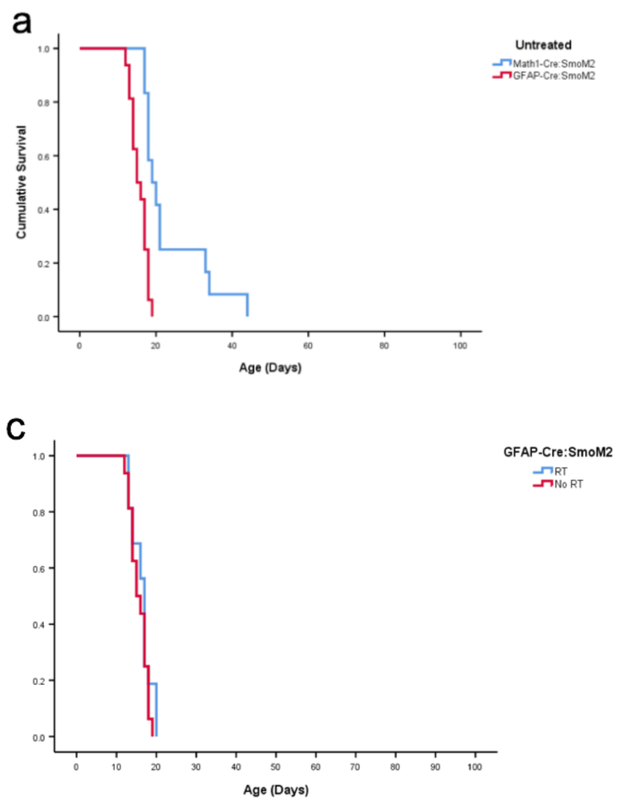

Fig. 2 Survival analysis of *M-Smo* and *G-Smo* mice. a) Kaplan-Meyer curve of untreated *M-Smo* and *G-Smo* mice (p = 0.00003, log-rank test) b) Kaplan-Meyer curve of untreated *M-Smo* and radiation treated *M-Smo* mice (p = 0.001) c) Kaplan-Meyer curve of untreated *G-Smo* and radiation treated *G-Smo* mice (p=0.275). P-values determined using log-rank test.

<u>Medulloblastomas from progenitors or stem cells exhibit differential cellular compositions</u>

We used single-cell RNA sequencing to identify differences between *M-Smo* and *G-Smo* medulloblastomas. We collected tumors at P15 from 5 *M-Smo* mice and 6 *G-Smo* mice and used the Drop-seq protocol to generate single cell transcriptomic profiles, collecting ~2,600 cells from each tumor (10, 11). We subjected the 11,984 *M-Smo* cells and 16,489 *G-Smo* cells to selection criteria as described in the Methods section in order to avoid keeping cells with insufficient read depths, cells that unintentionally have transcriptomic information from more than one cell, and premature lysis. After this filtering step, 5,930 *M-Smo* and 8,699 *G-Smo* were included in the analysis. As suggested by previous studies (12), to reduce batch effects in the analysis caused by different sequencing depths we randomly downsampled the *G-Smo* data by 60% to equate the sequencing depth to that of the *M-Smo* data.

We combined the *M-Smo* and *G-Smo* cells and used SCTransform to normalize the data and to identify the top 3,000 most variable genes. Following data normalization and variable gene selection, we used principal component analysis (PCA) to identify 16 principle components (PCs) that explain >77% of the variance in the 3,000 variable genes. We then used Louvain clustering to identify 20 clusters that represent groupings of transcriptionally similar cells. We used Uniform Manifold Approximation and Projection (UMAP) to reduce the dimensionality of the data for graphical visualization. We color-coded the cells by their cluster designation in the UMAP projection (fig. 3a). We generated lists of genes that are differentially expressed in each cluster compared to all other clusters to determine the biological validity and cell type of each cluster using Wilcoxon rank-sum test for significance.

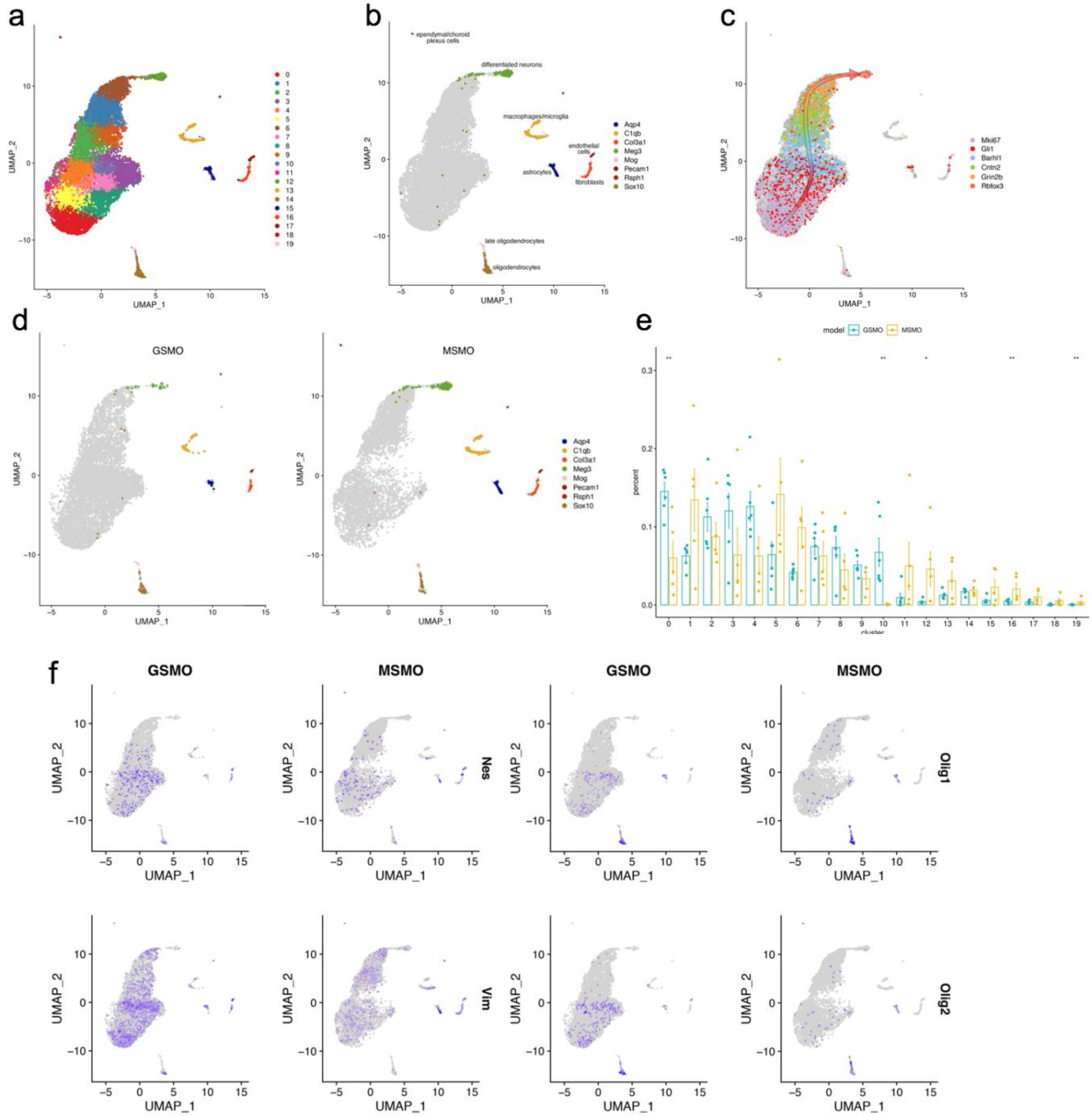

Fig. 3 Single-cell transcriptomic analysis of *M-Smo* and *G-Smo* tumors. a) UMAP projection of tumor cells from *M-Smo* and *G-Smo* mice color coded by clusters. b) Feature plot of stromal and neuronal markers. c) Feature plot of markers of CGNP development with an arrow indicating the axis of differentiation. d) Feature plot of stromal and neuronal markers separated by genotype. e) Fraction population of cells contributed by biological replicate to each cluster from *M-Smo* and *G-Smo* mice. * indicates p<.05 ** indicated p<.01 by Mann-Whitney U Test. f) Feature plot of *Nes*, *Vim*, *Olig1*, and *Olig2* separated by genotype.

Of the 20 clusters, we identified 8 clusters that are representative of tumor stroma using marker genes previously described (11,13-14). These stroma include astrocytes, oligodendrocytes, late oligodendrocytes, microglia/macrophages, fibroblasts, endothelial cells, neurons, and ciliated cells marked by expression of *Aqp4*, *Sox10*, *Mog*, *C1qb*, *Col3a1*, *Pecam1*, *Meg3,* and *Rsph1*, respectively (fig. 3b). The other clusters showed gene expression profiles mirroring those of CGNP development as described in (11), noting sequential expression of *Mki67*, *Gli1*, *Barhl1*, *Cntn2*, *Grin2b*, and *Rbfox3* representing the developmental axis from a proliferative to a differentiated state (fig. 3c).

To better understand the differences between *M-Smo* and *G-Smo* tumor cells, we plotted *M-Smo* and *G-Smo* derived cells separately, noticing that *M-Smo* derived CGNP-like cells differentially populate the differentiated end of the developmental axis while *G-Smo* derived cells differentially populate the proliferative end (fig. 3d). To quantify this difference, we calculated the number of cells a biological replicate has assigned to a given cluster divided by the total number of cells of that replicate (fig. 3e). We found that cluster 0 on the proliferative end was significantly enriched for *G-Smo* cells ($p = 0.0087$, Wilcoxon rank-sum test) while cluster 12 at the differentiated end is significantly enriched for *M-Smo* cells ($p = 0.017$). Cluster 10 is almost exclusively made up of *G-Smo* cells ($p = 0.0043$). In addition, there is an increased number of fibroblasts ($p = 0.0087$) and late oligodendrocytes ($p = 0.0043$) in *M-Smo* tumors. Together, these results show that *M-Smo* and *G-Smo* tumors have different cellular compositions, with *M-Smo* tumors having more differentiating cells than *G-Smo* tumors.

Cell state differences between *M-Smo* and *G-Smo* tumors within CGNP-like population

To better understand the characteristics of the *G-Smo* cells in clusters 0 and 10, we generated differential expression lists between the *G-Smo* cells in each cluster and the *M-Smo* CGNP-like tumor clusters. We found that Olig family genes *Olig1* and *Olig2* are increased in both clusters as well as stem cell marker genes *Nes* and *Vim* (fig. 3f). In addition, we also note the upregulation of eukaryotic elongation factor genes *Eef2*, *Eef1b2*, and *Eef1g* and ribosomal protein genes in cluster 10, which suggests these cells have an increased capacity for protein synthesis (15). In contrast, all the cells in cluster 12 show higher expression of *Gabra6* and *Meg3* when compared to all other cells in both tumor models, which are markers for differentiated cerebellar granule neurons (11, 16). *G-Smo* tumors are enriched for cells with stem cell phenotypes and an elevated capacity for protein synthesis while *M-Smo* tumors are enriched for differentiated neurons.

Stromal cell population differences between *M-Smo* and *G-Smo* tumors

To investigate the tumor microenvironment, we analyzed the stromal cells outside of the Gfap lineage, including macrophages/microglia and endothelial cells. In this analysis, we include cells from normal cerebellum collected at P7 to identify differences between tumor and normal stroma. We used the Harmony algorithm to combine the tumor and normal cerebellum datasets (17). We used the Harmony dimensional reduction to generate cell clusters and a UMAP projection as described previously. We identified stromal cells and neurons with the markers previously described (fig. 4a). We isolated the macrophage/microglia and endothelial cell clusters and subjected the cells to Harmony and clustering analysis. Following clustering, we generated differential gene lists for each cluster and quantified the contribution of each genotype to each cluster as described previously.

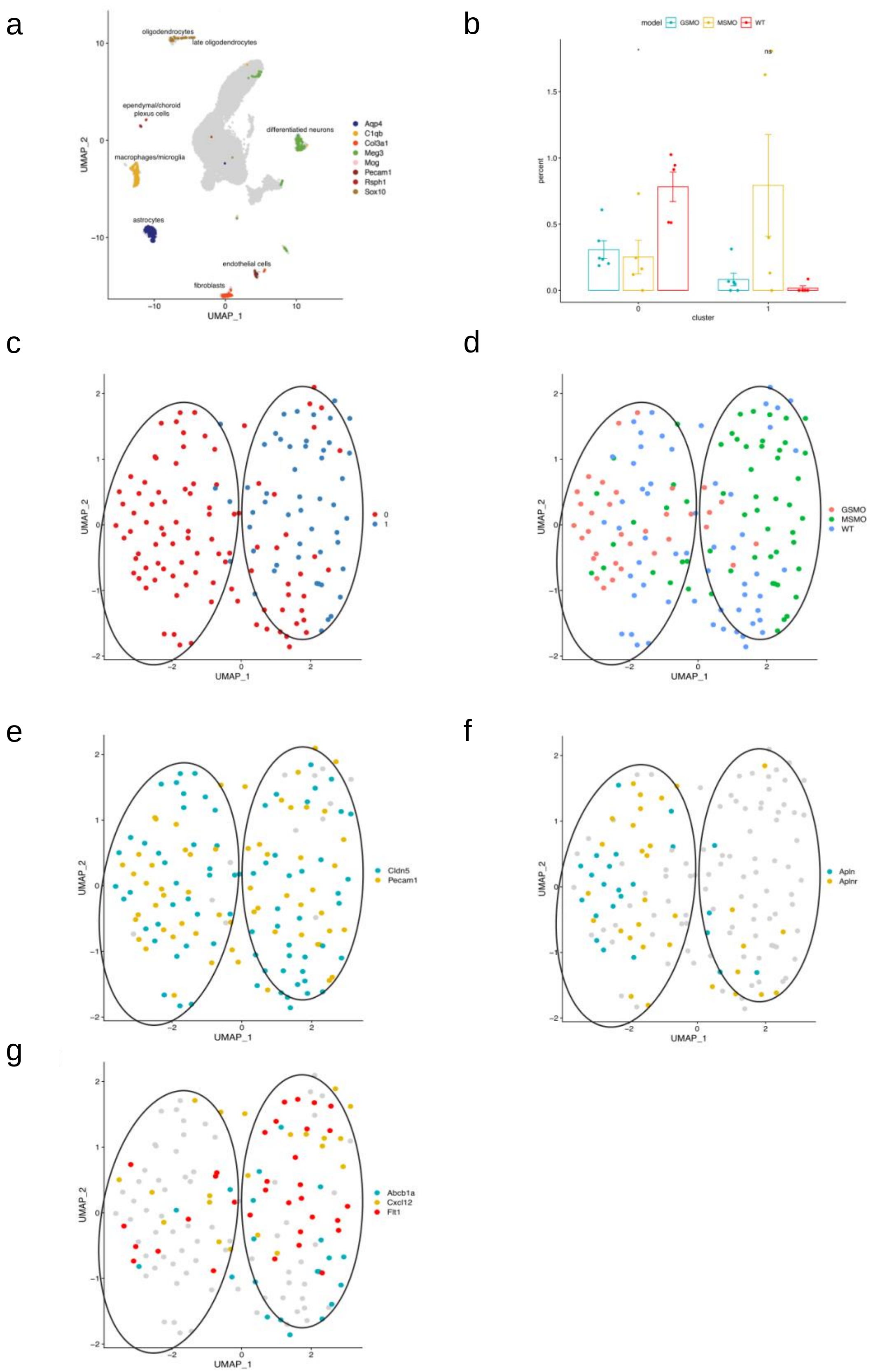
a
b
c
d
e
f
g
oligodendrocytes
late oligodendrocytes
ependymal/choroid plexus cells
differentiated neurons
macrophages/microglia
astrocytes
endothelial cells
fibroblasts
Aqp4
C1qb
Col3a1
Meg3
Mog
Pecam1
Rsph1
Sox10
UMAP_1
UMAP_2
model
GSMO
MSMO
WT
percent
cluster
ns
Cldn5
Pecam1
Apln
Aplnr
Abcb1a
Cxcl12
Flt1

Fig. 4 Single-cell transcriptomic analysis of of endothelial cells from *M-Smo* and *G-Smo* tumors combined with normal P7 cerebellum.

a) Feature plot of stromal and neuronal markers for *M-Smo* and *G-Smo* mice and normal P7 cerebellum. b) Fraction population of cells contributed by biological replicate to macrophage/microglia each cluster from *M-Smo* and *G-Smo* mice and normal P7 cerebellum. * indicates p<.05 ** indicated p<.01 by Kruskal-Wallis Test. c) UMAP projection of endothelial color coded by cluster and d) by genotype. Feature plots of e) general endothelial markers f) markers for cluster 0, and g) markers for cluster 1.

In the endothelial cell population, we identified 2 clusters (fig. 4b,c). Cluster 0 was common to both normal cerebellum and both tumor genotypes while cluster 1 was tumor-specific (fig. 4b,d). All endothelial cell clusters expressed marker genes *Cldn5* and *Pecam1* (fig. 4e). Cluster 0 showed upregulation of *Mki67* and *Apln*, suggesting that these are proliferative, developing endothelial cells (22) (fig. 4f). In contrast, cluster 1 showed an upregulation of *Abcb1a*, *Cxcl12*, and *Flt1*, which have both been associated with medulloblastoma pathogenesis and tumor neoangiogenesis, respectively (23-24) (fig. 4g). Thus, *M-Smo* and *G-Smo* tumors have a unique endothelial cell population that is associated with pro-tumoral properties. Collectively, these results show that *M-Smo* and *G-Smo* tumors have differential stromal population compositions as well as shared, tumor-specific stroma.

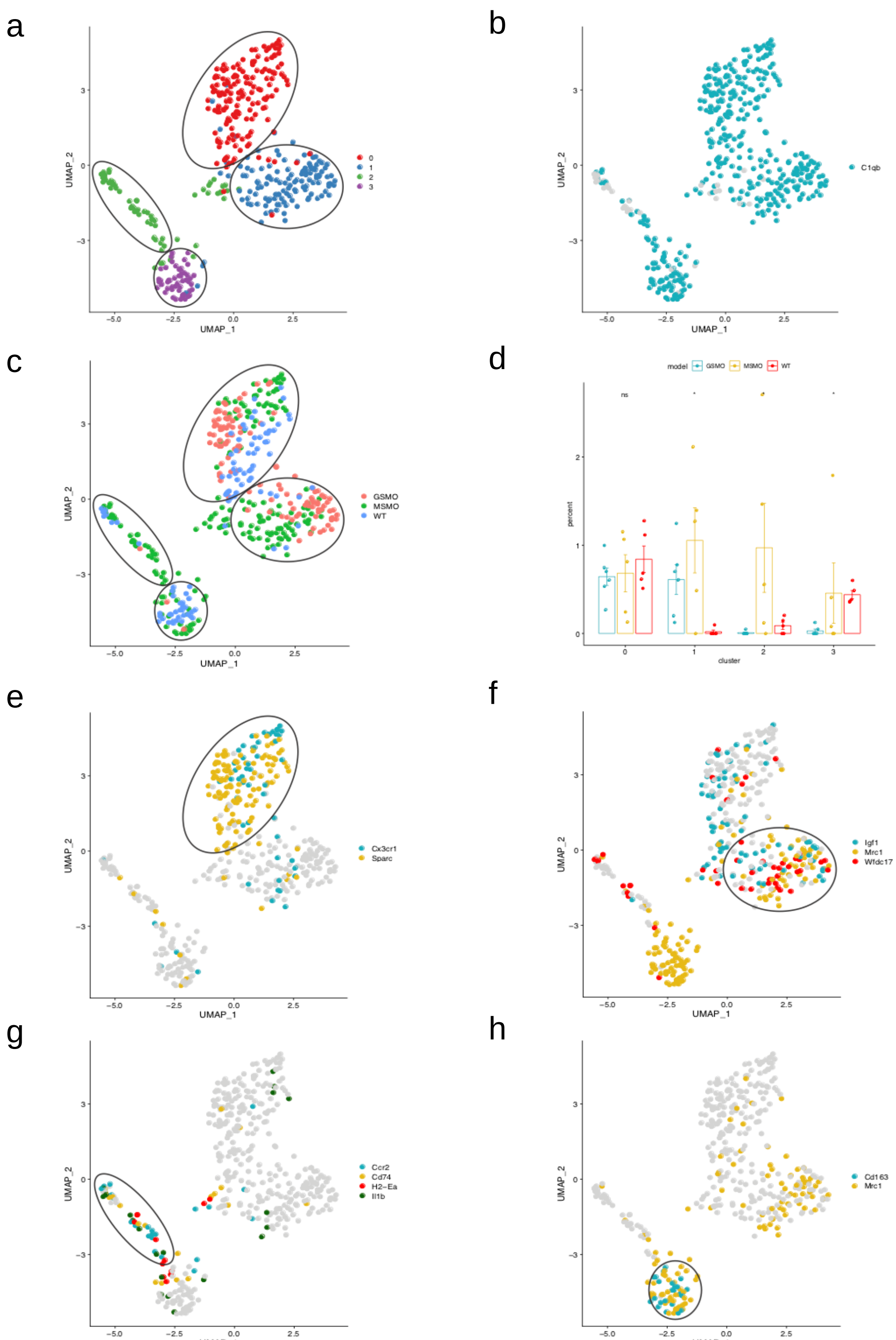
a
b
c
d
e
f
g
h
UMAP_1
UMAP_2
0
1
2
3
C1qb
GSMO
MSMO
WT
model
percent
cluster
ns
Cx3cr1
Sparc
Igf1
Mrc1
Wfdc17
Ccr2
Cd74
H2−Ea
Il1b
Cd163
Mrc1

Fig. 4 Single-cell transcriptomic analysis of of macrophage/microglia cells from *M-Smo* and *G-Smo* tumors combined with normal P7 cerebellum.

a) UMAP projection of macrophage/microglial cells color coded by cluster. b) general macrophage/microglia marker. c) UMAP projection of macrophage/microglial cells color coded by genotype. d) Fraction population of cells contributed by biological replicate to macrophage/microglia each cluster from *M-Smo* and *G-Smo* mice and normal P7 cerebellum. * indicates $p<.05$ ** indicated $p<.01$ by Kruskal-Wallis Test. Feature plots of markers for e) cluster 0, f) cluster 1, g) cluster 2, and h) cluster 3.

In the macrophage/microglia population, we identified 4 clusters (fig. 5a). All macrophage/microglial clusters expressed the general marker *C1qb* (fig. 5b). Cluster 0 was common to both normal cerebellum and both tumor genotypes, cluster 1 was tumor-specific, and clusters 2 and 3 were common to *M-Smo* tumors and wildtype cerebellum (fig. 5c,d). Cluster 0 was upregulated for *Cx3cr1* and *Sparc*, which is a gene expressed by mature microglia (18). Cluster 1 showed upregulation for *Mrc1*, *Igf1*, and *Wfdc17* (fig. 5e), suggesting that the cells comprising this cluster represent a mature M2-like macrophage population, which are thought to be immunosuppressive and tumorigenic (19). Cluster 2 was marked by higher expression of *Ccr2*, *Cd74*, *H2-Ea*, and *Il1b* indicating these are proinflammatory M1-like macrophages (20). Cluster 3 showed upregulation of *Cd163* and *Mrc1*, suggesting these are also an M-2 like macrophage population (21). These results show that *G-Smo* and *M-Smo* tumors have a macrophage population that is unique to tumors in comparison to wildtype cerebellum and that *M-Smo* tumors have a more diverse set of macrophages than *G-Smo* tumors.

Discussion

Our results suggest that timing of tumor initiation results in markedly different tumors with regards to their malignancy and response to therapy. This finding was reified by their differential cellular composition as shown by single-cell RNA sequencing. The *G-Smo* medulloblastoma tumors initiated earlier in development led to shorter survival time and increased resistance to radiation. These tumors have a larger fraction of stem-like cells and *Olig2+* cells. Cancer stem cells are important drivers of tumor progression (25), and *Olig2+* cells have recently been shown to be enriched in therapy resistant and recurrent medulloblastomas (26), suggesting that these cells may be implicated in the worse clinical outcomes observed in *G-Smo* tumors. In addition, we also found that there is a subset of *G-Smo* tumor cells that show an upregulation of ribosomal protein genes and eukaryotic elongation factors, which has been implicated in promoting tumorigenesis in various cancers (15). In contrast, *M-Smo* medulloblastoma tumors initiated later in development were enriched in fully differentiated neurons that are nonpropagating and are therefore not contributing to tumor growth.

In addition to differences in the main tumor population, we observed differential tumor-stromal interaction in the two tumor models as well as differences in stromal composition between the tumors and normal P7 cerebellum. *M-Smo* tumors proved to have a larger fraction of late oligodendrocytes and fibroblasts and to have a more diverse set of macrophage populations that are also present in normal cerebellum. *M-Smo* tumors have a unique M1-like macrophage population. M1 macrophages have been shown to have antitumor effects (21), suggesting that the *M-Smo*-specific population could be implicated in its reduced malignancy. We found that both tumors have a tumor-specific M2-like macrophage. As M2 macrophages are reported to have protumoral effects by suppressing the immune response (15), these macrophages may be an important population to target in the treatment of these tumors and further research should investigate their role in tumor progression. We also found a population of endothelial cells that is enriched in tumors. This endothelial population is marked by genes associated with medulloblastoma development and tumor growth (23). These tumor- and genotype-specific cell populations, along with the differentially enriched tumor cell populations, should be further studied with regards to their contribution to medulloblastoma growth and clinical outcomes so that targeted therapies can be developed against those populations implicated in increased tumor malignancy. Collectively, we have shown that the developmental timing of medulloblastoma initiation is an important predictor of tumor composition and clinical outcomes.

Methods

Mouse acquisition and Drop-seq protocol and data preprocessing of 5 *M-Smo* and 6 *G-Smo* tumors was conducted identically to the methods described in Ocasio et al. The code for the data analysis and visualization is available at: https://github.com/malawsky/Gershon_single-cell/blob/master/senior_thesis_code.

References

1. Northcott, P.A., Robinson, G.W., Kratz, C.P. et al. Medulloblastoma. Nat Rev Dis Primers. 2019;5(11).
2. Cavalli FMG, Remke M, Rampasek L, Peacock J, Shih DJH, Luu B, et al. Intertumoral Heterogeneity within Medulloblastoma Subgroups. Cancer Cell. 2017;31(6):737-54 e6.
3. Carballo, G.B., Honorato, J.R., de Lopes, G.P. et al. A highlight on Sonic hedgehog pathway. Cell Commun Signal 2018;16(11).
4. Oliver TG, Read TA, Kessler JD, Mehmeti A, Wells JF, Huynh TTT, et al. Loss of patched and disruption of granule cell development in a pre-neoplastic stage of medulloblastoma. Development. 2005;132(10):2425-39.
5. Yang Z-J, Ellis T, Markant SL, Read T-A, Kessler JD, Bourboulas M, et al. Medulloblastoma Can Be Initiated by Deletion of Patched in Lineage-Restricted Progenitors or Stem Cells. Cancer Cell. 2008;14(2):135-45.
6. Schüller U, Heine VM, Mao J, Kho AT, Dillon AK, Han Y-G, et al. Acquisition of Granule Neuron Precursor Identity Is a Critical Determinant of Progenitor Cell Competence to Form Shh-Induced Medulloblastoma. Cancer Cell. 2008;14(2):123-34.
7. Mao J, Ligon KL, Rakhlin EY, Thayer SP, Bronson RT, Rowitch D, et al. A Novel Somatic Mouse Model to Survey Tumorigenic Potential Applied to the Hedgehog Pathway. Cancer Research. 2006;66(20):10171-8.
8. Machold R, Fishell G. Math1 Is Expressed in Temporally Discrete Pools of Cerebellar Rhombic-Lip Neural Progenitors. Neuron. 2005;48(1):17-24.
9. Zhuo L, Theis M, Alvarez-Maya I, Brenner M, Willecke K, Messing A. hGFAP-cre transgenic mice for manipulation of glial and neuronal function in vivo. genesis. 2001;31(2):85-94.
10. Macosko, E. Z. et al. Highly parallel genome-wide expression profiling of individual cells using nanoliter droplets. Cell. 2015;161(5):1202–1214.
11. Ocasio J, Babcock B, Malawsky D, Weir SJ, Loo L, Simon JM, et al. scRNA-seq in medulloblastoma shows cellular heterogeneity and lineage expansion support resistance to SHH inhibitor therapy. Nat Commun. 2019;10(1):5829.

12. Luecken MD, Theis FJ. Current best practices in single-cell RNA-seq analysis: a tutorial. Mol Syst Biol. 2019;15(6):e8746.

13. Scolding NJ, Firth S, Linington C, et al. Myelin-oligodendrocyte glycoprotein (MOG) is a surface marker of oligodendrocyte maturation. J Neuroimmunol 1989;22(3):169-76.

14. Knowles M, Ostrowski L, Leigh M, et al. Mutations in RSPH1 Cause Primary Ciliary Dyskinesia with a Unique Clinical and Ciliary Phenotype. Am J Resp Crit Care.2014;189(6).

15. Ruggero, D., Pandolfi, P. Does the ribosome translate cancer?. Nat Rev Cancer 2003;3:179–192.

16. Wang W, Stock R, Gronostajki R, et al. A Role for Nuclear Factor I in the Intrinsic Control of Cerebellar Granule Neuron Gene Expression. J Bio Chem. 2004;279(51):53491-7.

17. Korsunsky I, Millard N, Fan J, Slowikowski K, Zhang F, Wei K, et al. Fast, sensitive and accurate integration of single-cell data with Harmony. Nat Methods. 2019;16(12):1289-96.

18. Vincent AJ, Lau PW, Roskams AJ. SPARC is expressed by macroglia and microglia in the developing and mature nervous system. Dev Dyn. 2008;237(5):1449-62.

19. Arlauckas S, Garren S, Garris C, Kohler R, Oh J, et al. Arg1 expression defines immunosuppressive subsets of tumor-associated macrophages. Theranostics. 2018;8(21):5842–54.

20. Avila M, Berasain C. Targeting CCL2/CCR2 in Tumor-Infiltrating Macrophages: A Tool Emerging Out of the Box Against Hepatocellular Carcinoma. Cell Mol Gast Hep. 2019;7(2):293-4.

21. Martinez F, Gordon S. The M1 and M2 paradigm of macrophage activation: time for reassessment. F1000Prime Rep. 2014;6(13).

22. Liu Q, Hu T, He L, Huang X, Tian X, et al. Genetic targeting of sprouting angiogenesis using Apln-CreER. Nat Comm. 2015;6(6020).

23. Ozawa PM, Ariza CB, Ishibashi CM, Fujita TC, et al. Role of CXCL12 and CXCR4 in normal cerebellar development and medulloblastoma. Int J Cancer. 2016;38(1):10-3.

24. Slongo M, Molena B, Brunati A, Frasson M, et al. Functional VEGF and VEGF receptors are expressed in human medulloblastomas. Neuro Oncol. 2007;9(4):384–92.

25. Ayob A, Ramasamy T. Cancer stem cells as key drivers of tumour progression. J Bio Sci. 2018;25(20).

26. Zhang L, He X, Liu X, Zhang F, Huang L, et al. Single-Cell Transcriptomics in Medulloblastoma Reveals Tumor-Initiating Progenitors and Oncogenic Cascades during Tumorigenesis and Relapse. Cancer Cell. 2019;3(36):302-18.